Multiple feature-enhanced SAR imaging using sparsity in combined dictionaries

Sadegh Samadi [1], Müjdat Çetin [2], Mohammad Ali Masnadi-Shirazi [3]

[1]Department of Electrical and Electronics Engineering, Shiraz University of Technology, Modarres Blvd., 71557-13876 Shiraz, Iran.

[2]Faculty of Engineering and Natural Sciences, Sabanci University, Tuzla, 34956 Istanbul, Turkey.

[3]School of Electrical and Computer Engineering, Shiraz University, Zand Street, 71348-51154 Shiraz, Iran.

ABSTRACT

Non-quadratic regularization based image formation is a recently proposed framework for feature-enhanced radar imaging. Specific image formation techniques in this framework have so far focused on enhancing one type of feature, such as strong point scatterers, or smooth regions. However, many scenes contain a number of such feature types. We develop an image formation technique that simultaneously enhances multiple types of features by posing the problem as one of sparse signal representation based on combined dictionaries. Due to the complex-valued nature of the reflectivities in SAR, this method is developed based on the sparse representation of the *magnitude* of the scattered field , composed of appropriate dictionaries associated with different types of features. The multiple feature-enhanced reconstructed image is then obtained through a joint optimization problem over the combined representation of the magnitude and the phase of the underlying field reflectivities. We also present some considerations on the combined dictionary selection and propose an efficient combined dictionary for specific features of interest in a radar image. We demonstrate the effectiveness of this method through experimental results and quantify the quality of the reconstructed images based on a number of image quality metrics.

Keywords: synthetic aperture radar, multiple feature enhancement, sparse signal representation, combined dictionary, image reconstruction, complex valued imaging, overcomplete dictionary.

1. INTRODUCTION

The all weather, day and night, high resolution capabilities make synthetic aperture radar (SAR) an ideal remote sensing system for many applications. The anticipated high data rates and the time critical nature of emerging SAR tasks motivate the use of automated processing techniques in extracting information from a

SAR image for an accurate and efficient interpretation of the scene. There is growing interest in such techniques, wherein features extracted from the formed imagery are used for tasks such as automatic target detection and recognition. The conventional image formation algorithms in traditional SAR systems are based on the Fourier transform [1], which leads to images limited in resolution by the system bandwidth, and exhibiting noise and side lobe artifacts. This kind of processing does not take into account either any available contextual information, or the final objectives of the SAR mission regarding the automated decisions or interpretations to be made.

Recently significant effort has been spent towards new approaches for SAR image formation. An important motivation for these approaches has been improving the resolution beyond the Fourier limit, which has resulted in the development of a number of superresolution methods. These methods contain a wide spectrum of techniques such as subspace projection techniques [2], parameter estimation or spectral estimation techniques [3,4], and data extrapolation techniques [5]. The essence of these methods is the consideration of some parametric models for SAR images or underlying targets and considering the SAR image formation as a parameter estimation problem. Most of these methods consider a model that assumes that the underlying field can be considered as a combination of point scatterers. Therefore most of these image formation approaches enhance point like features of the underlying fields, however reduce gain on non-point like features, and they usually fail to enhance shape based features of images containing distributed targets [6].

Non-quadratic regularization based image formation is a recently proposed framework for feature-enhanced radar imaging [6]. This framework offers a number of advantages over conventional imaging including superresolution, robustness to uncertain or limited data, and enhanced image quality in non-conventional data collection scenarios such as sparse aperture sensing. This method uses an ill-posed linear model which regards the true pixel values of the complex-valued undegraded image as unknown parameters. Specific image formation techniques in this framework have so far focused on enhancing one type of feature in the imaged scene, such as strong point scatterers, or regions with smoothly varying reflectivities. However, many scenes contain, and hence require joint enhancement of, a number of such feature types.

In this paper we develop an image formation technique that simultaneously enhances multiple types of features in the scene. By viewing the image formation problem as a sparse signal representation problem,

similar in spirit to [7] but in combined dictionaries, this is achieved by using appropriate dictionaries that combine multiple types of features. In particular, we consider dictionary combinations that jointly represent spatially focused and spatially distributed scene features. The mathematical formulation of this problem is developed in this paper and multiple feature-enhanced reconstructed images are obtained through a joint optimization over the combined representation of the magnitude and the phase of the complex-valued undegraded image. Our experimental analysis demonstrates the improvements provided by this approach. Section 2 provides the details of our mathematical framework as well as our solution to the optimization problems encountered in this framework. Section 3 presents our experimental results and conclusions are presented in Section 4.

2. THE FRAMEWORK OF MULTIPLE FEATURE ENHANCED SAR IMAGING

This section describes our mathematical formulation for multiple feature enhanced SAR imaging. As we explained, recent techniques such as nonquadratic regularization [6], have mostly focused on enhancement of one type of feature in the process of image formation. Improvements achieved by these methods are the result of using prior information about the scene of interest. This information is incorporated by putting some penalties on the image to be reconstructed from the sampled received data. When the scene is believed to contain multiple types of features (e.g., isolated scatterers and spatially distributed objects), then the approach in [6] appears to suggest adding terms corresponding to each type of feature into the overall cost function to be optimized for imaging. However, this may result in a potentially undesired effect, as multiple and potentially inconsistent constraints could be imposed over the same spatial region.

Recently, a technique for SAR imaging based on sparse signal representation has been developed [7]. This work, which introduces the sparse representation (SR) approach for the complex-valued inverse problem of SAR image formation, has shown the capability of SR approach for producing high quality SAR images as well as exhibiting robustness to uncertain or limited data. Extending this work, here a framework for multiple feature enhanced SAR imaging is developed based on sparse representation of the magnitude of the scattered field in terms of appropriate dictionaries associated with different types of features.

2.1 SAR observation model

Two common observation models for SAR imaging problem which have been used in the literature are the geometric theory of diffraction (GTD) based model and the ill-posed linear model. The former which is

motivated by both physical optics and the geometric theory of diffraction regards the target scattering centers and amplitudes as parameters of a point scattering model [8]. The latter which is motivated by tomographic formulation of SAR regards the complex-valued undegraded image of the underlying scene as unknown. The GTD-based model has mostly been used in superresolution methods which have successfully improved point like features of the underlying field. However, this model is not a good choice for methods that are intended to enhance (e.g., shape based) features of distributed targets as the model is not rich in this regard.

In recent works [6,7], the ill-posed linear model has successfully been used in methods that improve non-point like features of distributed targets, so here we use this model which provides an appropriate basis for our purpose of enhancing multiple types of features in the reconstructed image. In particular the linear, noisy observation model used in this paper is given by:

$$\mathbf{g} = \mathbf{H}\,\mathbf{f} + \mathbf{n} \tag{1}$$

where $\mathbf{g}$ is the sampled range profile, $\mathbf{f}$ is the undegraded radar image of the underlying scene, and $\mathbf{n}$ is the observation noise; all are column-stacked as vectors and of complex-valued nature. $\mathbf{H}$ represents the ill-posed discrete SAR projection operator [6].

2.2 Sparsity in combined dictionaries

Consider M features to be enhanced simultaneously in the process of SAR image formation. Though the unknown scene $\mathbf{f}$ in our observation model is complex-valued, in most applications we are interested in features of its magnitude [7]. So our approach is based on sparse representation of the magnitude in a combination of appropriate dictionaries:

$$\left|\mathbf{f}\right| = \sum_{i=1}^{M} \mathbf{\Phi}_i \boldsymbol{\alpha}_i \tag{2}$$

where $\mathbf{\Phi}_i$'s are appropriate dictionaries for our application that can sparsely represent the scene in terms of the features of interest, and $\boldsymbol{\alpha}_i$'s are vectors of representation coefficients. We can write:

$$\mathbf{f} = \mathrm{diag}\{\boldsymbol{\beta}\}\left|\mathbf{f}\right| = \mathrm{diag}\{\left|\mathbf{f}\right|\}\boldsymbol{\beta} \tag{3}$$

where $\boldsymbol{\beta}$ is a vector with elements $(\boldsymbol{\beta})_i = \beta_i = e^{j\phi_i}$, and ϕ_i is the unknown phase of $(\mathbf{f})_i$. Substituting (2) and (3) into (1) we obtain :

$$y = \sum_{i=1}^{M} \mathbf{H} \operatorname{diag}\{\boldsymbol{\beta}\} \boldsymbol{\Phi}_i \boldsymbol{\alpha}_i \; + \mathbf{n} = \mathbf{H} \operatorname{diag}\{|\mathbf{f}|\} \boldsymbol{\beta} + \mathbf{n} \tag{4}$$

Considering $\boldsymbol{\beta}$ to be known for now, an estimate of $\boldsymbol{\alpha}_i$'s can be found through the following extended basis pursuit-like method [9]:

$$\{\hat{\boldsymbol{\alpha}}_1, ..., \hat{\boldsymbol{\alpha}}_M\} = \arg \min_{\boldsymbol{\alpha}_1, ..., \boldsymbol{\alpha}_M} \left\| \mathbf{y} - \sum_{i=1}^{M} \mathbf{H} \operatorname{diag}\{\boldsymbol{\beta}\} \boldsymbol{\Phi}_i \boldsymbol{\alpha}_i \right\|_2^2 + \sum_{i=1}^{M} \lambda_i \|\boldsymbol{\alpha}_i\|_{p_i}^{p_i} \tag{5}$$

where $\|\cdot\|_p$ denotes the ℓ_p-norm, and λ_i's are positive real parameters. We have let $p_i \leq 1$, for $i=1,...,M$ to be different so that we can choose proper values according to the ability of each dictionary $\boldsymbol{\Phi}_i$ to sparsely represent the corresponding feature of interest.

Now considering $|\mathbf{f}|$ (or equivalently $\boldsymbol{\alpha}_i$'s) to be known, an estimate of $\boldsymbol{\beta}$ can be obtained through the following estimator [7]:

$$\hat{\boldsymbol{\beta}} = \arg \min_{\boldsymbol{\beta}} \left\| \mathbf{y} - \mathbf{H} \operatorname{diag}\{|\mathbf{f}|\} \boldsymbol{\beta} \right\|_2^2 + \lambda' \sum_{i=1}^{N^2} (|(\boldsymbol{\beta})_i| - 1)^2 \tag{6}$$

where N^2 is the number of elements of vector $\boldsymbol{\beta}$ for an image of size $N \times N$. For the actual problem where both the $\boldsymbol{\alpha}_i$'s and $\boldsymbol{\beta}$ are unknown, we define the following multivariate cost function:

$$J_t(\boldsymbol{\alpha}_1, ..., \boldsymbol{\alpha}_M, \boldsymbol{\beta}) = \left\| \mathbf{y} - \sum_{i=1}^{M} \mathbf{H} \operatorname{diag}\{\boldsymbol{\beta}\} \boldsymbol{\Phi}_i \boldsymbol{\alpha}_i \right\|_2^2 + \sum_{i=1}^{M} \lambda_i \|\boldsymbol{\alpha}_i\|_{p_i}^{p_i} + \lambda' \sum_{i=1}^{N^2} (|(\boldsymbol{\beta})_i| - 1)^2 \tag{7}$$

The estimates of $\boldsymbol{\alpha}_i$'s and $\boldsymbol{\beta}$, hence that of the complex-valued image can be obtained through the following block coordinate descent approach:

$$\{\hat{\boldsymbol{\alpha}}_1^{(l+1)}, ..., \hat{\boldsymbol{\alpha}}_M^{(l+1)}\} = \arg \min_{\boldsymbol{\alpha}_1, ..., \boldsymbol{\alpha}_M} J_t(\boldsymbol{\alpha}_1, ..., \boldsymbol{\alpha}_M, \hat{\boldsymbol{\beta}}^{(l)}) \tag{8}$$

$$\hat{\boldsymbol{\beta}}^{(l+1)} = \arg \min_{\boldsymbol{\beta}} J_t(\hat{\boldsymbol{\alpha}}_1^{(l+1)}, ..., \hat{\boldsymbol{\alpha}}_M^{(l+1)}, \boldsymbol{\beta}) \tag{9}$$

where l denotes the iteration index.

2.3 Iterative solution of the block coordinate descent algorithm

The partial gradient of the multivariate cost function $J_t(\boldsymbol{\alpha}_1, ..., \boldsymbol{\alpha}_M, \boldsymbol{\beta})$ with respect to $\boldsymbol{\alpha}_i$ is:

$$\nabla_{\boldsymbol{\alpha}_i} J_t(\boldsymbol{\alpha}_1, ..., \boldsymbol{\alpha}_M, \boldsymbol{\beta}) = \mathbf{G}_i(\boldsymbol{\alpha}_i) \, \boldsymbol{\alpha}_i - 2(\mathbf{H} \operatorname{diag}\{\boldsymbol{\beta}\} \boldsymbol{\Phi}_i)^H (\mathbf{y} - \sum_{\substack{j=1 \\ j \neq i}}^{M} \mathbf{H} \operatorname{diag}\{\boldsymbol{\beta}\} \boldsymbol{\Phi}_j \boldsymbol{\alpha}_j) \tag{10}$$

where
$$\mathbf{G}_i(\boldsymbol{\alpha}_i) = 2\,(\mathbf{H}\,\mathrm{diag}\{\boldsymbol{\beta}\}\boldsymbol{\Phi}_i)^H\,(\mathbf{H}\,\mathrm{diag}\{\boldsymbol{\beta}\}\boldsymbol{\Phi}_i) + \lambda_i\,p_i\,\boldsymbol{\Lambda}(\boldsymbol{\alpha}_i) \tag{11}$$

and
$$\boldsymbol{\Lambda}(\boldsymbol{\alpha}_i) = \mathrm{diag}\left\{\frac{1}{\left(\left|(\boldsymbol{\alpha}_i)_k\right|^2 + \varepsilon\right)^{1-p_i/2}}\right\} \tag{12}$$

in which ε is a small positive constant used to avoid the nondifferentiability problem of the ℓ_p-norm around the origin, and $(\boldsymbol{\alpha}_i)_k$'s are the elements of the vector $\boldsymbol{\alpha}_i$. Rewriting the gradient terms in (10) for i=1,…,M in matrix form, we reach to the following result:

$$\begin{bmatrix} \nabla_{\boldsymbol{\alpha}_1} J_t(\boldsymbol{\alpha}_1,...,\boldsymbol{\alpha}_M,\boldsymbol{\beta}) \\ \nabla_{\boldsymbol{\alpha}_2} J_t(\boldsymbol{\alpha}_1,...,\boldsymbol{\alpha}_M,\boldsymbol{\beta}) \\ \vdots \\ \nabla_{\boldsymbol{\alpha}_M} J_t(\boldsymbol{\alpha}_1,...,\boldsymbol{\alpha}_M,\boldsymbol{\beta}) \end{bmatrix} = \begin{bmatrix} \mathbf{G}_1(\boldsymbol{\alpha}_1) & 2\,(\mathbf{H}\,\mathrm{diag}\{\boldsymbol{\beta}\}\boldsymbol{\Phi}_1)^H (\mathbf{H}\,\mathrm{diag}\{\boldsymbol{\beta}\}\boldsymbol{\Phi}_2) & \cdots & 2\,(\mathbf{H}\,\mathrm{diag}\{\boldsymbol{\beta}\}\boldsymbol{\Phi}_1)^H (\mathbf{H}\,\mathrm{diag}\{\boldsymbol{\beta}\}\boldsymbol{\Phi}_M) \\ 2\,(\mathbf{H}\,\mathrm{diag}\{\boldsymbol{\beta}\}\boldsymbol{\Phi}_2)^H (\mathbf{H}\,\mathrm{diag}\{\boldsymbol{\beta}\}\boldsymbol{\Phi}_1) & \mathbf{G}_2(\boldsymbol{\alpha}_2) & \cdots & 2\,(\mathbf{H}\,\mathrm{diag}\{\boldsymbol{\beta}\}\boldsymbol{\Phi}_2)^H (\mathbf{H}\,\mathrm{diag}\{\boldsymbol{\beta}\}\boldsymbol{\Phi}_M) \\ \vdots & \vdots & \ddots & \vdots \\ 2\,(\mathbf{H}\,\mathrm{diag}\{\boldsymbol{\beta}\}\boldsymbol{\Phi}_M)^H (\mathbf{H}\,\mathrm{diag}\{\boldsymbol{\beta}\}\boldsymbol{\Phi}_1) & 2\,(\mathbf{H}\,\mathrm{diag}\{\boldsymbol{\beta}\}\boldsymbol{\Phi}_M)^H (\mathbf{H}\,\mathrm{diag}\{\boldsymbol{\beta}\}\boldsymbol{\Phi}_2) & \cdots & \mathbf{G}_M(\boldsymbol{\alpha}_M) \end{bmatrix}$$
$$\begin{bmatrix} \boldsymbol{\alpha}_1 \\ \boldsymbol{\alpha}_2 \\ \vdots \\ \boldsymbol{\alpha}_M \end{bmatrix} - \begin{bmatrix} 2\,(\mathbf{H}\,\mathrm{diag}\{\boldsymbol{\beta}\}\boldsymbol{\Phi}_1)^H\,\mathbf{y} \\ 2\,(\mathbf{H}\,\mathrm{diag}\{\boldsymbol{\beta}\}\boldsymbol{\Phi}_2)^H\,\mathbf{y} \\ \vdots \\ 2\,(\mathbf{H}\,\mathrm{diag}\{\boldsymbol{\beta}\}\boldsymbol{\Phi}_M)^H\,\mathbf{y} \end{bmatrix} \tag{13}$$

or equivalently :
$$\nabla_{\widetilde{\boldsymbol{\alpha}}} J_t(\widetilde{\boldsymbol{\alpha}},\boldsymbol{\beta}) = \widetilde{\mathbf{G}}(\widetilde{\boldsymbol{\alpha}})\,\widetilde{\boldsymbol{\alpha}} - \widetilde{\mathbf{y}} \tag{14}$$

in which $\widetilde{\boldsymbol{\alpha}} = \begin{bmatrix} \boldsymbol{\alpha}_1^T & \cdots & \boldsymbol{\alpha}_M^T \end{bmatrix}^T$. Note that $\widetilde{\mathbf{G}}$ in (14) is a function of $\widetilde{\boldsymbol{\alpha}}$ and we can not find a closed form solution for $\widetilde{\boldsymbol{\alpha}}$. Using $\widetilde{\mathbf{G}}(\widetilde{\boldsymbol{\alpha}})$ as an approximation to the Hessian, the following quasi-Newton algorithm can be used to solve the optimization problem in (8) iteratively at each step l (we ignore reference to l here for the sake of notational simplicity):

$$\hat{\widetilde{\boldsymbol{\alpha}}}^{(n+1)} = \hat{\widetilde{\boldsymbol{\alpha}}}^{(n)} - [\widetilde{\mathbf{G}}(\hat{\widetilde{\boldsymbol{\alpha}}}^{(n)})]^{-1}\,\nabla J(\hat{\widetilde{\boldsymbol{\alpha}}}^{(n)}) \tag{15}$$

Substituting (14) into (15), the following iterative algorithm is obtained:

$$\widetilde{\mathbf{G}}(\hat{\widetilde{\boldsymbol{\alpha}}}^{(n)})\,\hat{\widetilde{\boldsymbol{\alpha}}}^{(n+1)} = \widetilde{\mathbf{y}} \tag{16}$$

Note that l denotes the iteration index of the overall block coordinate descent algorithm for minimizing the cost function in (7), and n denotes the iteration index of the algorithm for solving the subproblem in (8) for each l. Taking the partial gradient of $J_t(\boldsymbol{\alpha}_1,...,\boldsymbol{\alpha}_M,\boldsymbol{\beta})$ with respect to $\boldsymbol{\beta}$ and continuing in a similar way to the above procedure we can find the following iterative algorithm for solving the optimization problem in (9):

$$\mathbf{G}'(\hat{\boldsymbol{\beta}}^{(n)})\,\hat{\boldsymbol{\beta}}^{(n+1)} = 2\,(\mathbf{H}\,\mathrm{diag}\{|\mathbf{f}|\})^H\,\mathbf{y} \tag{17}$$

where
$$\mathbf{G}'(\boldsymbol{\beta}) = 2\,(\mathbf{H}\,\mathrm{diag}\{|\mathbf{f}|\})^H\,(\mathbf{H}\,\mathrm{diag}\{|\mathbf{f}|\}) + 2\,\lambda'\left(\mathbf{I} - \mathrm{diag}\left\{\frac{1}{|(\boldsymbol{\beta})_i|}\right\}\right) \tag{18}$$

2.4 Considerations on combined dictionary selection

The above framework allows the use of combinations of various dictionaries based on the features to be enhanced simultaneously. Two features that we are usually interested in SAR images are strong point scatterers of man-made targets and smooth regions of different natural regions in the terrain or distributed targets. To select a dictionary we should consider both its ability to sparsely represent the feature of interest and the likelihood of efficient implementation of the above algorithm using it. We introduce the following two combined dictionaries with these characteristics for enhancing simultaneously point-like targets and smooth areas in SAR images.

2.4.1 Point and region-based (PR) dictionary

The shape based dictionary (SB) introduced in [7] could be a good candidate for this purpose however, it is not computationally efficient. Here we propose a simpler dictionary which is much more efficient. This dictionary is a combination of two subdictionaries: a point-based subdictionary and a region-based subdictionary. The point-based subdictionary is a dictionary of isolated point scatterers at all possible positions. Considering our formulation in the previous sections, for a SAR image of size $N\times N$, the size of this subdictionary is $N^2\times N^2$. More specifically it is an identity matrix of this size. For the region-based subdictionary we propose to use a dictionary or a combination of various dictionaries of local spatial smoothing filters for enhancing smooth regions in the image. Each column of such a dictionary contains elements of an $N\times N$ matrix, with all elements zero except for a local region around a specific pixel, reshaped as a vector. Therefore, each atom in this dictionary takes the shape of the impulse response of a low-pass spatial filter, centered around a particular pixel. Different types of smoothing filters can be used based on the features of the smooth region of interest. Averaging, circular averaging, low pass Gaussian filters, inverse of approximate local Laplacian operator are examples of such local space smoothing filters. The size of each of these region-based subdictionaries is $N^2\times N^2$, and any combination of them can be used when it is necessary.

2.4.2 Spike-Contourlet (SC) dictionary

This dictionary is also composed of two subdictionaries. For the point-like scatterers the best dictionary, as we mentioned above, is a dictionary of shifted unit samples at every possible location in a fixed grid in the

scene of interest. Curvelet is a powerful dictionary for sparse representation of smooth regions. However, its non-orthogonality and the large number of output coefficients make it very inefficient for implementation of our algorithm. Contourlet is an orthogonal type curvelet without the large number output coefficients problem. We can also efficiently implement our algorithm using this dictionary. Therefore, spike-contourlet is a proper combined dictionary for joint enhancement of point-like targets and smooth regions in SAR images.

PR and SC dictionaries are just samples of appropriate combined dictionaries to show the abilities of the new approach and any such combined dictionary can be used in this framework. One can try to find other combined dictionaries for different applications.

3. EXPERIMENTAL RESULTS

In this section, we demonstrate the validity of the proposed method on both synthetic and real SAR scenes containing multiple types of features. We compare our results with conventional polar format imaging [1] and point-region-enhanced nonquadratic regularization [6] to show the improvements achieved. To compare the reconstructed images quantitatively we use the following quality metrics for real SAR scenes where we do not have the true ground image.

a. Target to clutter ratio (TCR): as a measure of enhancement of point-like targets with respect to the background [11,12]:

$$\text{TCR} = 20 \, \log_{10} \left(\frac{\max_{i \in \mathcal{T}} \left(|(\hat{\mathbf{f}})_i| \right)}{\frac{1}{N_c} \sum_{j \in c} |(\hat{\mathbf{f}})_j|} \right) \tag{19}$$

where $\mathcal{T}$ is the target region, c is the clutter region and N_c denotes the number of pixels in the clutter region.

b. Mainlobe width (MLW): as defined in [12], which is a measure of the effective resolution and can be considered as a quality metric for point-like target enhancement.

c. Entropy of the full image (ENT) [13]: entropy can be used to measure the smoothness of the probability density function of image intensities. The smoother the distribution is, the larger the entropy is [13]. So an image with smooth regions (sharp distribution) has low entropy. Therefore, entropy can be considered as a quality metric for images with enhanced smooth regions.

d. Average speckle amplitude (ASA) [12]: speckle complicates description of smooth regions in conventional SAR images. A measure for speckle is the standard deviation of a clutter region in the dB-valued SAR image [11,12].

e. Mean target edge strength (MTES): as defined in [14]: "The Sobel operator is used to generate the edge map. Then the average of all edge magnitudes above a minimum threshold is denoted as the mean target edge strength measure". Images with enhanced smooth regions should have higher values of MTES.

For synthetic scenes where the ground truth is known we use the Signal to Noise Ratio (SNR) and Target Localization Metrics as defined in [7].

3.1 Synthetic scene experiment

To demonstrate the capabilities of this new method and contrast it with existing methods, we consider a synthetic scene composed of both point targets and distributed targets, as shown in Fig. 1(a). The point targets have relatively smaller magnitudes than the distributed objects, and neither conventional imaging nor nonquadratic regularization could clearly distinguish them from the background. The reconstructed images in Fig. 1(c) and Fig. 1(d) show the success of the proposed approach in simultaneous enhancement of the two existing features in the scene. The quality metrics depicted in Table 1 show the achieved improvement quantitatively.

3.2 Experiment with ADTS data

In this experiment we use a scene from the MIT Lincoln Laboratory Advanced Detection Technology Sensor (ADTS) data set [10]. It is a natural scene of size 128×128 containing trees and a corner reflector. Fig. 1(a) shows the conventional reconstruction of this data which involves a rather poor display of the objects and regions in the scene, mostly due to severe speckle noise. The nonquadratic reconstruction of the scene is shown in Fig. 1(b) in which there is a tradeoff between enhancement of the two features of interest, namely the spatially-localized point reflectors, and the spatially distributed trees and regions. Fig. 1(c) and Fig. 1(d) show the reconstructed images based on the presented approach with PR and SC dictionaries in which both the corner reflector and the smooth distributed targets (trees) are very well enhanced simultaneously. Computed quality metrics depicted in Table 2 show the superiority of the proposed method over the nonquadratic regularization method in terms of all quality metrics.

In order to see the effect of dictionary selection and the need for the combined dictionary presented in this paper, Fig. 3 shows the reconstructed image using the contourlet dictionary. This dictionary can sparsely represent smooth regions and cannot do the same for point-like targets. Hence, the use of such a dictionary for scenes containing man-made targets may result in unacceptable reconstructions just like the one shown in Fig. 3.

4. CONCLUSIONS

In this paper we have considered the multiple feature enhanced SAR image reconstruction problem. We have developed an approach based on sparse representation of the magnitude of the complex-valued scattered field in terms of multiple features using a combination of appropriate dictionaries. The mathematical framework has been developed by extending the one in [7] and an iterative solution has been presented too. Selection of an appropriate combined dictionary so that we can implement efficiently the algorithm is very important. We have demonstrated the use of a sample combined dictionary for enhancing two specific features in radar images and one can try to propose other combined dictionaries for other features or applications. The reconstructed images presented in experimental results and evaluations based on the quality metrics demonstrate the effectiveness of the method to enhance simultaneously multiple feature types.

ACKNOWLEDGMENTS

REFERENCES

[1] W. G. Carrara, R. S. Goodman, and R. M. Majewski, *Spotlight Synthetic Aperture Radar: Signal Processing Algorithms*. Boston, MA: Artech House, 1995.

[2] S. Barbarosa, "SAR super-resolution imaging by signal subspace projection technologies," *AEU Int. J. Elect. Commun.*, vol. 50, no. 2, pp. 133–138, 1996.

[3] D. Pastina, A. Farina, J. Gunning, and P. Lombardo, "Two-dimensional superresolution spectral analysis applied to SAR images," *IEE Proc., Radar, Sonar, Navig.*, vol. 145, no. 5, pp. 281–290, 1998.

[4] S. R. Degraaf, "SAR imaging via modern 2D spectral estimation methods," *IEEE Trans. Imaging Process.*, vol. 7, no. 5, pp. 729–761, May 1998.

[5] A. E. Brito, S. H. Chan, and S. D. Cabera, "SAR image superresolution via 2-D adaptive extrapolation," *Multidimensional Syst. Signal Process.*, vol. 14, pp. 83–104, 2003.

[6] M. Çetin and W. C. Karl, "Feature-enhanced synthetic aperture radar image formation based on nonquadratic regularization," *IEEE Trans. Image Processing*, vol. 10, no. 4, pp. 623–631, Apr. 2001.

[7] S. Samadi, M. Çetin, and M. A. Masnadi-Shirazi, "Sparse Representation-Based SAR Imaging, " *IET Radar, Sonar & Navig.*, vol. 5, no. 2, pp. 182-193, Feb. 2011.

[8] M. J. Gerry, L. C. Potter, I. J. Gupta, and A. van der Merwe, "A parametric model for synthetic aperture radar measurements," *IEEE Trans. Antennas Propagat.*, vol. 47, no. 7, pp. 1179–1185, Jul. 1999.

[9] S. Chen, D. Donoho, and M. Saunder, "Atomic decomposition by basis pursuit," *SIAM J. Sci. Comput.*, vol. 20, pp. 33–61, 1998.

[10] Air Force Research Laboratory, Model Based Vision Laboratory, Sensor Data Management System ADTS. [Online] available: http://www.mbvlab.wpafb.af.mil/public/sdms/datasets/adts/.

[11] G. R. Benitz, "High-definition vector imaging," *Lincoln Laboratory Journal*, vol. 10, no. 2, pp. 147–170, 1997.

[12] M. Çetin, W.C. Karl, and D. A. Castañon, "Feature enhancement and ATR performance using non-quadratic optimization-based SAR imaging," *IEEE Trans. Aerospace and Electronic Systems*, vol. 39, no. 4, pp. 1375-1395, 2003.

[13] J. Wang and X. Liu, "SAR minimum-entropy autofocus using an adaptive-order polynomial model," *IEEE Trans. Geoscience and Remote Sensing*, vol. 3, no. 4, pp. 512-516, 2006.

[14] Y. Chen, G. Chen, R.S. Blum, E. Blasch, and R. S. Lynch, "Image quality measures for predicting automatic target recognition performance," *IEEE Aerospace Conference*, March 2008, pp.1-9.
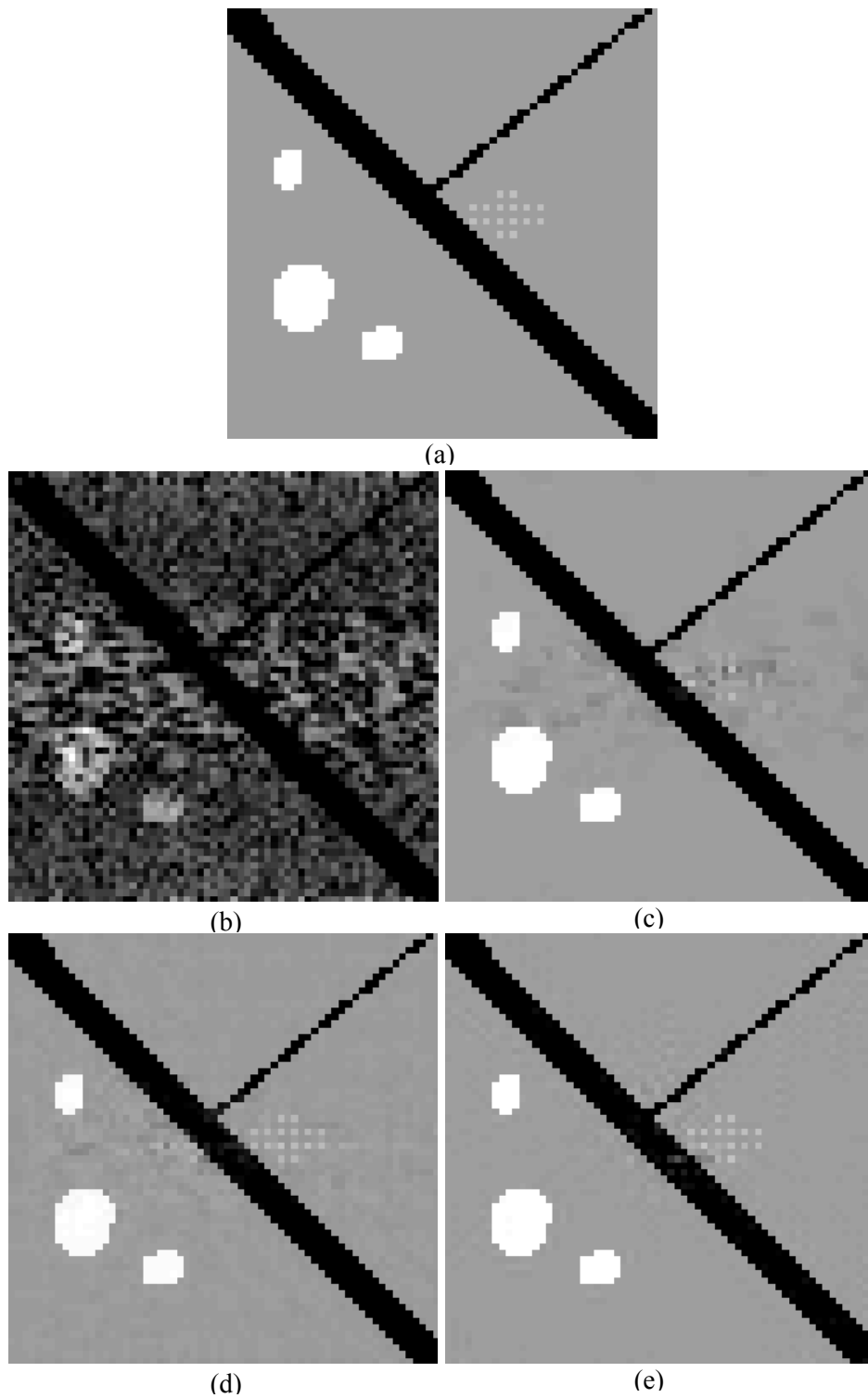
Fig. 1. Synthetic scene reconstructions   (a) synthetic scene,   (b) conventional reconstruction,   (c) point-region-enhanced nonquadratic regularization, (d) Proposed approach with PR dictionary,   (e) Proposed approach with SC dictionary.
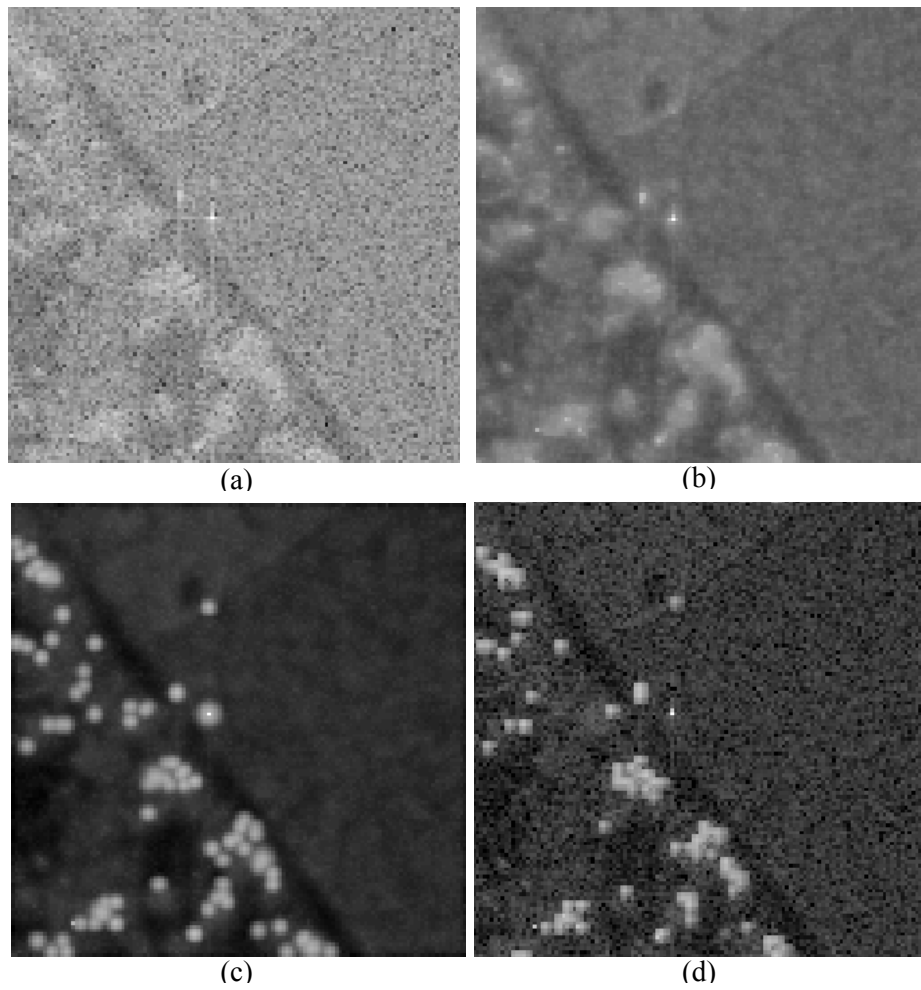
Fig. 2. Results with the ADTS data (a) conventional reconstruction, (b) point-region-enhanced (nonquadratic regularization) reconstruction, (c) Reconstruction of the proposed approach with PR dictionary, (d) Reconstruction of the proposed approach with SC dictionary.
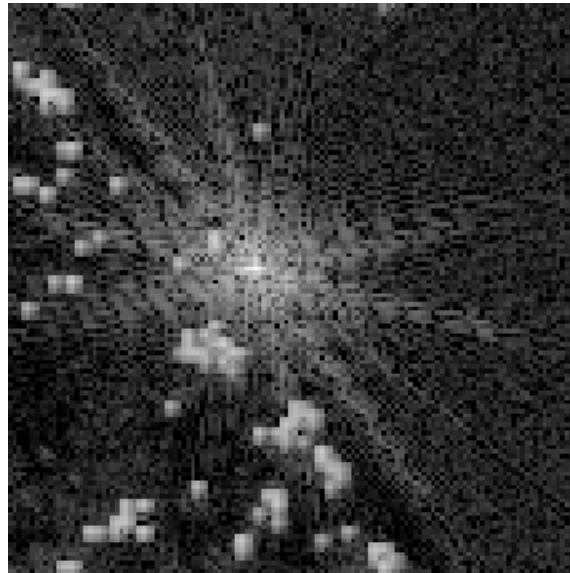
Fig. 3. Reconstruction of the ADTS data using the contourlet dictionary.

Table1 Computed quality metrics for reconstructed images shown in Fig. 1.

	Conventional	Nonquadratic	Proposed Method (PR)	Proposed Method (SC)
SNR(dB)	14.44	28.52	30.15	31.53
TLM(%)	90.40	99.38	99.43	99.53

Table 2 Computed quality metrics for reconstructed images shown in Fig.2

	Conventional	Nonquadratic	Proposed Method (PR)	Proposed Method (SC)
TCR, dB	36.23	53.50	58.77	69.18
MLW, m	0.319	0.630	0.601	0.355
ENT	3.418	0.721	0.516	0.406
ASA, dB	3.636	0.588	0.243	0.297
MTES	0.010	0.015	0.027	0.020